Shock Waves (2003) 13: 375–384
Digital Object Identifier (DOI) 10.1007/s00193-003-0179-0

Shock Waves

Development of some hypersonic benchmark flows using CFD and experiment

R. Hillier[1], R.R. Boyce[2], S.A. Creighton[1], A. Fiala[1], A.P. Jackson[3], S.G. Mallinson[4], A.H. Sheikh[1], S. Soltani[5], S. Williams[1]

[1] Imperial College of Science, Technology and Medicine, London, UK
[2] ADFA, University of New South Wales, Australia
[3] Aircraft Research Association, Bedford, UK
[4] Silverbrook Research, Balmain, NSW, Australia
[5] Renault, Mecanique des Fluides et Combustion, France

Received 10 October 2001/ Accepted 19 November 2002
Published online 4 February 2003 –

Abstract. This paper presents a set of test cases in high speed aerodynamics that describe our perceived relationship between experiment and computation. Computational fluid dynamics, with sensible interpretation, can guide experimental design, so that wind tunnel studies can focus better on fundamental 'benchmark' studies. Likewise experimental data may be used as feed back to evaluate codes and to improve their physical modelling. Here we present several test cases, developed in our laboratory, that we regard as basic 'building blocks' for high speed aerodynamics. These include: design for boundary-layer/pressure-gradient interaction; cavity flows; shock-wave/boundary-layer interactions; techniques for a graduated and controlled study of three-dimensional separated flows.

Key words: Hypersonic, CFD, Experiment, Benchmark cases
PACS: 47.40.Ki, 47.11.tj, 47.85.Gj, 47.32.Ff

1 Introduction

High speed aerodynamics presents a particularly demanding research area, experimentally and computationally, so that there is a special advantage in integrating the two approaches as closely as possible. Measurement of many quantities is difficult or impossible, and model manufacture is expensive and time-consuming. Thus CFD can assist in configuration development, either in terms of the overall geometry or in the detail of the location of expensive and sensitive instrumentation, and can 'probe' flow field areas or flow properties that are not accessible to experiments. This does not require unquestioned belief in the accuracy of CFD modelling, however. CFD faces many problems in efficient and accurate algorithm development/implementation (e.g providing adequate mesh density in sensitive flow areas and time-accurate resolution for unsteady flows) and in the flow physics (e.g. turbulence modelling, transition modelling, reaction modelling etc.) so that experiments should both investigate flow physics and also support code development and evaluation. These 'validation' or 'assessment' or experiment/CFD 'partnership' issues have been the subject of many papers and workshops (e.g. Rizzi and Vos 1998; Oberkampf 2000; Vos et al. 2001). Because of the progressive expansion in CFD, experiments increasingly need to be designed as 'benchmark' studies to provide specific high quality data against which CFD codes might be assessed. This paper therefore focusses mainly on efforts in our laboratory to combine CFD and experiments for a set of 'building block' investigations. These reflect our specific interests and are directed to boundary layer dominated flows including: 'controlled' studies of the effects of increasingly severe pressure gradient on turbulent boundary layer development; shock-induced separations; cavity flows; imposition of 'controlled' three-dimensionality on separated flows.

Correspondence to: R. Hillier (r.hillier@ic.ac.uk)
An abridged version of this paper was presented at the 23rd Int. Symposium on Shock Waves at Fort Worth, Texas, from July 22 to 27, 2001

2 The computational method

Most details of the CFD approach are available (Jackson et al. 2001; Hillier et al. 1995), so that only the main points are repeated here. The method uses 'convection-diffusion' splitting, solving the convective (i.e. Euler) terms using an explicit second-order upwind Godunov-type solver and evaluating the diffusive (viscous) terms with either centred differencing and implicit time integration, for thin layer

Navier Stokes formulation, or Runga-Kutta integration for full Navier Stokes. The resultant solver is second order accurate, in space and time, in smooth regions. An ideal equation of state for nitrogen (the experimental test gas) is used, together with the following formulation (Keyes 1952) for the temperature dependence of the molecular viscosity (kg/m/s),

$$\mu = \frac{1.418 \times 10^{-6} T^{1/2}}{1 + 116.4 T^{-1} 10^{-5/T}} \; . \qquad (1)$$

Constant Prandtl numbers of 0.72 and 0.9 are used in laminar and turbulent regions respectively and all simulations assume isothermal wall conditions (appropriate for a short-duration facility where temperature changes are small) with a wall temperature $T_w = 293$ K.

The turbulence models that are available in the code are simple, with options of an algebraic eddy viscosity model (Baldwin and Lomax 1978), one-equation variants of the $k - \epsilon$ model (Baldwin and Barth 1990; Goldberg and Ramakrishnan 1994; Menter 1997) and the Launder-Sharma formulation of the two-equation $k - \epsilon$ linear eddy viscosity model (Patel et al. 1985; Wilcox 1992). Apart from the Baldwin-Barth model, which seems to require a high initial turbulence 'seeding' level and shows excessive dependence upon mesh resolution, all the remaining models produce comparable predictions for attached boundary layer flows. For CFD design these are probably adequate. For high quality modelling, however, there are probably strong reasons for moving to non-linear eddy viscosity and Reynolds stress transport models (e.g. Hasan and McGuirk 2001) though little serious assessment is available for high Mach number flows. Compressibility corrections are a complex issue and are not fully understood, but nonetheless some formulations are relatively simple and effective (e.g. Shyy and Krishnamurty 1997). Our turbulent results are presented here without any compressibility correction, though a test with the Wilcox model (Wilcox 1992) produces about a 15% reduction in surface heat transfer for the attached boundary layer.

3 The wind tunnel & instrumentation

The test facility is a gun tunnel, operating with nitrogen gas at a nominal Mach number of 9 and a total temperature in the range of 1000 K to 1150 K – essentially 'cold hypersonics'. The operating unit Reynolds numbers range approximately from 9 million per metre to 47 million per metre. Model lengths up to a maximum of 0.9 m are posible, so that experiments can range from laminar studies to flows with 'natural' transition and extended lengths of turbulent flow. An earlier tunnel calibration exercise (Mallinson et al. 2000) was undertaken to ensure that flow initialisation conditions for the CFD can be specified as precisely as possible and includes the effects of (slight) test section axial gradients and flow angularity. In our tunnel the highest unit Reynolds number test condition produces the severest axial Mach number gradient, an increase of approximately 2.7% over one metre. This corresponds to a 19% fall in static pressure; significant for long models, but easily accommodated in the flow initialisation conditions for CFD modelling. At the lowest unit Reynolds number conditions, used for some laminar cavity flow studies, the test section flow is in effect uniform within calibration accuracy over the model length. Table 1 provides flow and calibration data for the tunnel for these two conditions. The total flow duration is 20 ms, of which about 5 ms is taken as the steady flow window. The data presented here are either surface pressure measurements, using miniature Kulite transducers positioned just below the model surface at the end of short tappings to minimise response times, or thin-film platinum resistance-gauges (on MACOR) for heat transfer measurement with temperature histories reduced digitally using the method due to Cook and Felderman (Cook and Felderman 1966, Schultz and Jones 1973). The measurement accuracy is assessed as $\pm 4\%$ and $\pm 7\%$ for pressure and heat transfer respectively.

4 The test problems

To study two-dimensional flow fields we regard it as natural to employ bodies of revolution since it is possible to establish high quality two-dimensional axisymmetric flows whereas *nominally* two-dimensional planar flows are always contaminated to some extent by side constraint effects, especially so once flow separation occurs. Thus our two-dimensional studies have used bodies of revolution and our three-dimensional studies have been based upon some controlled departure from the reference axisymmetric flow. Of course, use of an axisymmetric configuration cannot, by itself, guarantee two-dimensionality. A strong, fixed trailing vortex system – Taylor-Goertler-type vortices – has been shown to form downstream of an axisymmetric rearward-facing step in a supersonic flow (Roshko and Thomke 1966) and, as we will also note later, it is believed that cellular Taylor-Goertler systems can form in cavity flows (Jackson et al. 2001). Nevertheless, these features are fundamental aspects of the flow physics, rather than a coincidental, and uncontrolled, consequence of side constraints.

4.1 Configuration design for turbulent boundary layer in adverse pressure gradients (high unit Reynolds number case)

The first test concerns the configuration design for the systematic study of turbulent boundary layers in the presence of a family of adverse pressure gradients of increasing severity, developed for the high unit Reynolds number condition of Table 1. The reference zero pressure gradient (zpg) boundary layer is generated on a long (up to 850 mm chord), hollow circular cylinder (75 mm outer diameter and 50 mm inner diameter, with a chamfered leading edge) aligned axially with the flow (see Fig. 1), the model exterior providing the test surface. This reference boundary layer is then acted-on by the pressure gradient which, for

Table 1. Test section flow conditions for 'Low' and 'High' unit Reynolds number operation

M_∞	dM_∞/dx (%/m)	$P0_\infty$ (bar)	$T0_\infty$ (K)	T_{wall} (K)	Re_∞(/metre)
8.9 (± 0.5%)	0	98 (±2%)	1000 (±4%)	293 (±2%)	9,540,000 (±6%)
8.9 (± 0.5%)	2.7	600 (±2%)	1150 (±4%)	293 (±2%)	47,400,000 (±6%)

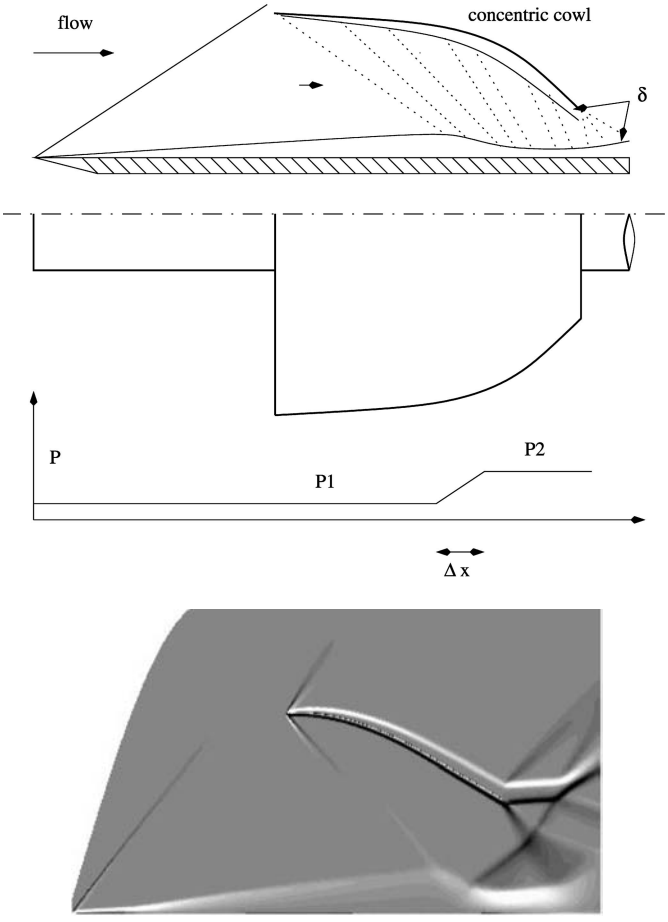

Fig. 1. Type 2 device for generating adverse pressure gradients. Schematic (not to scale) of hollow cylindrical body, used to generate zpg boundary layer, plus concentric cowl. CFD density field (stretched radial scale) for one of the designs

axisymmetric flows, can be generated either by geometric modification of the centrebody (Type 1 – curved wall device) or by use of an external compression cowl (Type 2, see the schematic of Fig. 1) to produce a reflected wave system on the centrebody without significant curvature of the test flow. A similar principle has been used in other studies for concave walls (Donovan et al. 1994) and for reflected wave systems (Kussoy et al. 1978; Fernando and Smits 1990; Smith and Smits 1996). As a *minimum* design constraint we would wish to specify the required pressure ratio through the interaction and also the severity and profile of the gradient. Figure 2 shows a demonstration for the Type 1 interaction, in this case with the constraints that a specified *constant* pressure gradient (cpg) is 'switched-on' as abruptly as possible from the initial zero pressure gradient forebody flow (zpg), switched to zpg after a pressure ratio of 3:1 has been achieved, then switched to an equal, but opposite, favourable pressure gradient (fpg) until recovery back to the initial pressure is accomplished. The pressure gradient is first imposed at the 600 mm chord position, so that upstream of this location the body y-ordinate is therefore fixed at 37.5 mm, the cylinder outer radius. This computation, performed with the Menter one-equation variant (Menter 1997) of the $k-\epsilon$ turbulence model, requires an iterative procedure to converge to the required shape for the specified pressure distribution. It should be noted that the initial boundary layer thickness, and its resultant reduction through the severe pressure gradient, provides a very significant displacement thickness contribution to the interaction, so that a purely inviscid design would be entirely inadequate. It is not possible to converge exactly to the specified target distribution – the required abrupt 'switch-on' and 'switch-off' of the gradients are unrealistic in this respect – but the figure shows how closely the target has been realised. One important CFD requirement was to maintain adequate mesh resolution throughout the interaction. Thus the mesh was adapted interactively to provide at all streamwise locations: 160 cells from the body surface to the trace of the (weak) shock wave from the centrebody leading edge; approximately 80 mesh points from the surface to the boundary layer 'edge' (here defined, arbitrarily, as the location where the local shear stress is 0.5% of the wall value); a y^* value of 0.5 for the cell adjacent to the wall. These are all important constraints, since the boundary layer thickness reduces substantially through a severe compression interaction and without care the boundary layer resolution can easily switch from good to inadequate. As yet we have neither completed this 'flare' investigation as a full CFD parameter study nor performed any experimental tests. Instead, our main pressure gradient investigation (Mallinson et al. 1999) has focussed on Type 2, the use of an external, concentric pressure gradient cowl, shown in schematic in Fig. 1 together with flow field density contours from one of the CFD solutions. The practical advantage of this configuration, experimentally, is that only one set of instrumentation is required on the centrebody irrespective of the number of cowls tested; in contrast, for the Type 1 case, each centrebody profile region would require its own specific (and time-consuming to manufacture) instrumentation insert. The design exercise is more difficult, however, because of the remoteness of the cowl from the test surface. The target pressure distribution is shown in schematic in Fig. 1 and we again set various design specifi-

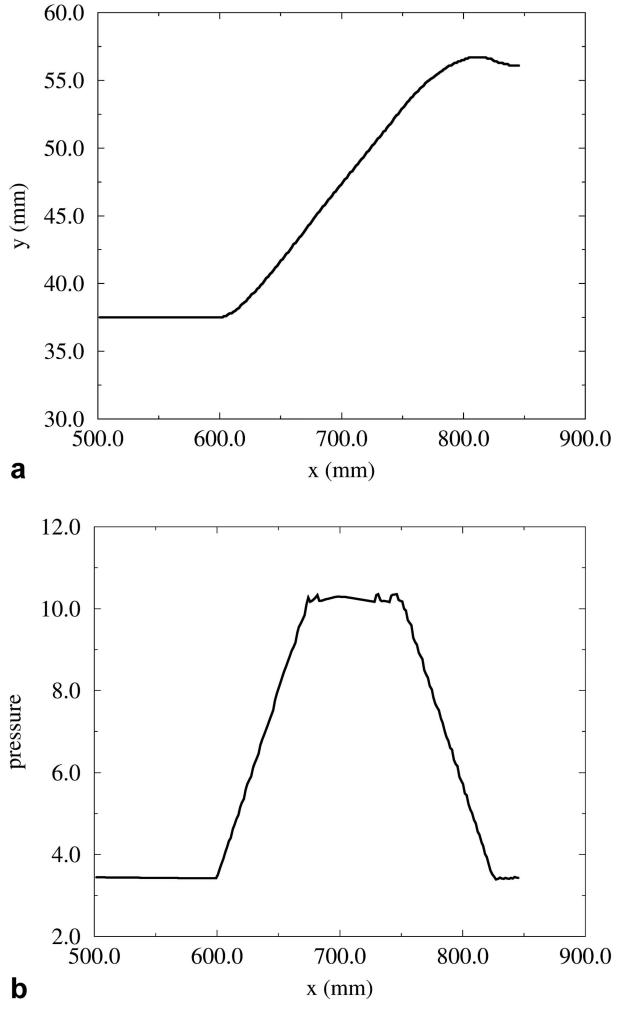

Fig. 2. Geometric shape **a** and computed pressure **b** for Type 1 (curved wall) device

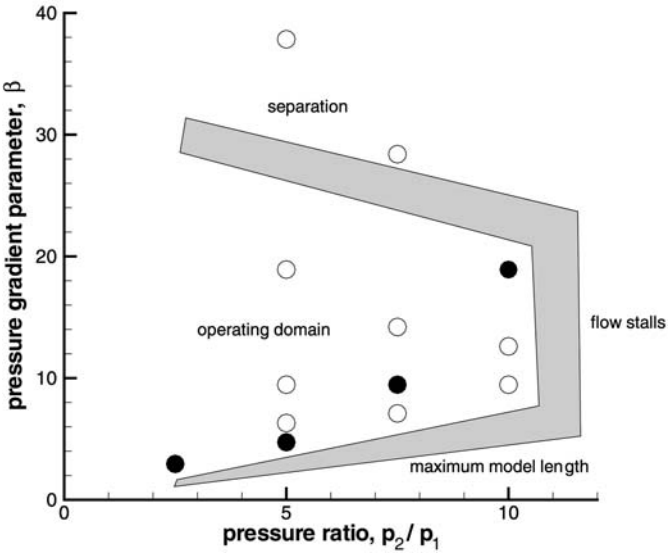

Fig. 3. Operating domain for the pressure gradient cowl designs. Open and solid symbols represent CFD simulations; solid symbols represent designs that were subsequently manufactured and tested

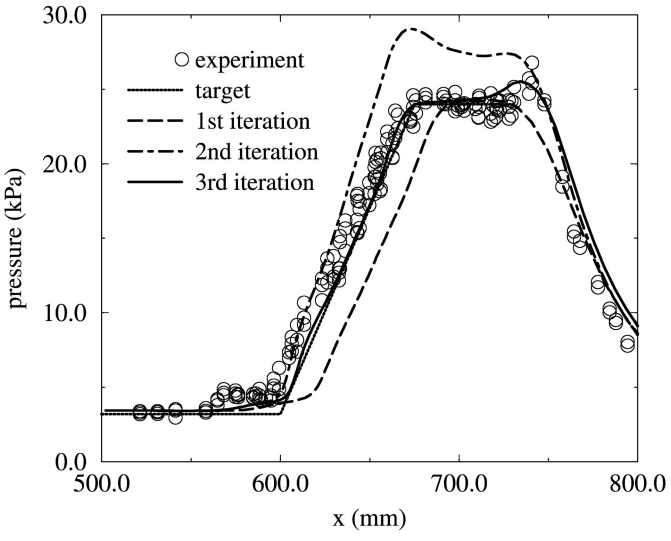

Fig. 4. Pressure gradient cowl design. CFD design iterations, and final measured pressure distribution, for 7.5:1 pressure ratio case

cations including: rapid 'switch-on' and 'switch-off' of the pressure gradient; development of a family of constant adverse pressure gradient designs up to the severest possible without producing flow separation; large overall pressure ratios. These were explored by CFD to produce the approximate operating domain of adverse pressure gradient versus total pressure ratio shown in Fig. 3.

The envelope to the domain is controlled therefore by separation, the physical available length of the model, and whether or not the tunnel starting flow can be swallowed by the cowl-centrebody annulus. The pressure gradient parameter β in Fig. 3 is a Clauser-type parameter, given as $\beta = (\delta^*/\tau_w)\, dp/dx$ (Laderman 1980), where the boundary layer displacement thickness, δ^*, and wall shear stress, τ_w, are evaluated just upstream of separation. A range of cowls were modelled by CFD, to give an approximate envelope to the operating domain, and four specific designs were subsequently manufactured and tested. The sequence of manufacture and tests was in the order of increasing pressure ratio (and pressure gradient), moving the designs progressively towards the expected limits of flow stalling/flow separation. Figure 4 presents a design sequence for the 7.5:1 pressure ratio, showing the 'target' distribution, plus a three-stage design iteration. The third and final one of these was constructed and the measured test data are included on the figure. This shows a very satisfactory design for a severe pressure gradient case, apart from some difficulty in controlling the initial switch-on of the pressure rise. This is largely associated with the design procedure attempting to 'cancel' the viscous interaction compression wave system radiated from the cowl leading edge.

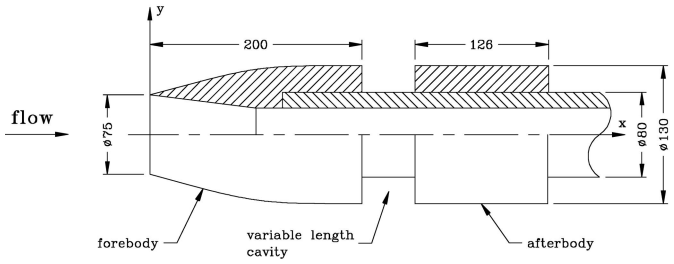

Fig. 5. Schematic for the axisymmetric cavity geometry, with dimensions in mm. The cavity depth is 25 mm and the length is variable

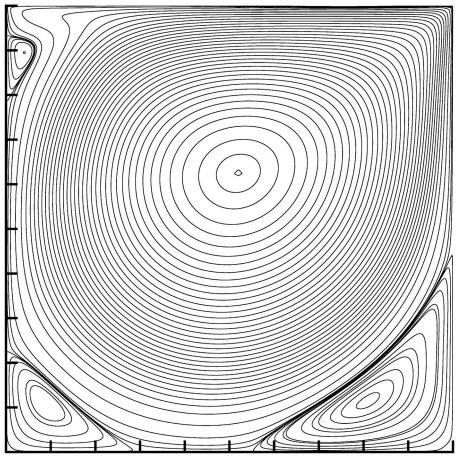

Fig. 6. Axisymmetric cavity with length-to-depth ratio, L/D, of 1.0 showing predicted streamlines

4.2 Design for two-dimensional laminar cavity flow (low unit Reynolds number case)

The results of this study have been extensively reported in Jackson et al. 2001, so that only the main points related to the CFD design will be referred to here. Cavity flows are of practical interest at hypersonic and at lower speeds. They provide a convenient CFD case since (for rectangular cavities at least) there is the option of using a simple mesh and the separation is more-or-less fixed at the leading edge of the cavity so that mesh refinement requirements can be well-focussed to capture separation correctly.

The configuration used is shown Fig. 5. Several practical design constraints were enforced. *Firstly*, the requirement for flow two-dimensionality automatically implied use of axisymmetric models as argued earlier. *Secondly*, the study was to be both laminar and turbulent (the latter is not reported here) and ensuring that laminar flow could be established presented a demanding requirement. A short forebody length was required (we used 200 mm), coupled with testing at our lowest unit Reynolds number condition. Data presented earlier (Jackson et al. 2001) clearly confirm both that the boundary layer at separation is indeed laminar and also that the flow is laminar on the afterbody downstream of the cavity. *Thirdly*, we wished there to be only a minimal pressure gradient imposed by the forebody on the cavity flow itself, so that ideally the forebody should be cylindrical or as close to cylindrical as possible. This automatically means that a *hollow* body of revolution would be required, which then presents a problem of flow starting. If the ratio of inlet diameter, to internal passage diameter, is too large the tunnel starting-wave system will not be 'swallowed', so that the flow instead becomes established with a detached shock wave in front of the model. The permitted diameter ratio was determined by simple tunnel tests with the outcome that, taking regard of the required cavity depth, a cylindrical forebody was not possible. The forebody was therefore designed by CFD with a profile such that the pressure would fall monotonically from the leading edge and establish a zero pressure gradient condition before the leading edge of the cavity is reached. *Fourthly*, the two main factors that determined the cavity depth were flow establishment times (see later) and the need for good data resolution. Both of these of course are in conflict, the response time considerations requiring a shallow cavity and the resolution considerations requiring a deep one. The final decision to use a 25 mm deep cavity was based on the fact that it was the deepest that we believed would still provide flow establishment during the short test time.

The computational domain covers the complete flow field, extending in the radial direction to just outboard of the trace of the bow shock wave (so that the far field boundary condition was a simple imposition of the free stream conditions) and in the axial direction for 350 mm from the leading edge (that is for 125 mm downstream of the cavity for the case reported here). A systematic procedure was followed to assess mesh refinement and the data presented here correspond to the finest of the simulations which, to all intents, can be regarded as mesh independent. The CFD converged to a *steady* state solution, though there are ample data for supersonic/hypersonic flows, however, to show that other cavity cases can produce strongly oscillatory behaviour (e.g. Morgenstern and Chokani 1994, Zhang et al. 1998, Tam et al. 1996).

Figure 6 presents the predicted steady-state streamline pattern for the cavity with a length-to-depth ratio, L/D, of 1.0. It is not possible to measure the cavity velocity field experimentally, or to measure the separation and reattachment positions for the predicted secondary separations. Because the predicted separation streamline follows virtually a straight line, effectively directly bridging the top of the cavity, it was pointed out (Jackson et al. 2001) that there are close links with low speed 'lid-driven' cavity flows. The secondary separation patterns predicted here are virtually identical to those obtained, at comparable Reynolds numbers, in the lid-driven case (e.g. Aidun et al. 1991, Ramanan and Homsy 1994). Figure 7 and Fig. 8 show comparisons between measurement and computation of heat transfer on the cavity floor and wall, as well as the immediately adjacent segments of the forebody and afterbody. Heat transfer is chosen as the quantity for comparison, since it is a sensitive measure of assessment for CFD codes. Data are presented as a wetted distance, S, along the body surface, referenced to zero at the cavity rear lip, and normalised by the cavity depth, D. Thus the floor of the cavity lies in the range $-2 \leq S/D \leq -1$,

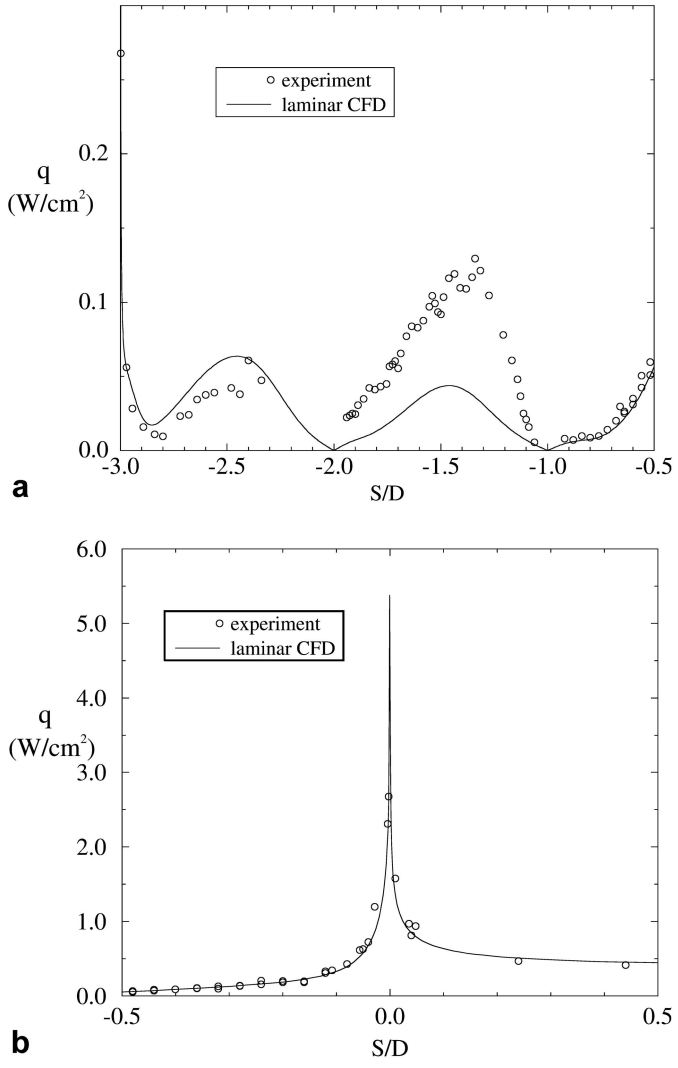

Fig. 7a,b. Comparison of computed and measured surface heat transfer rates for the cavity with L/D = 1. The wetted distance along the cavity and body surfaces is referenced to zero at the rearmost lip. **a** data in the interval from the forward cavity lip ($S/D = -3$) to the mid-height of the rear face of the cavity ($S/D = -0.5$). **b** data in the interval from the mid-height of the cavity back face to the afterbody downstream of reattachment

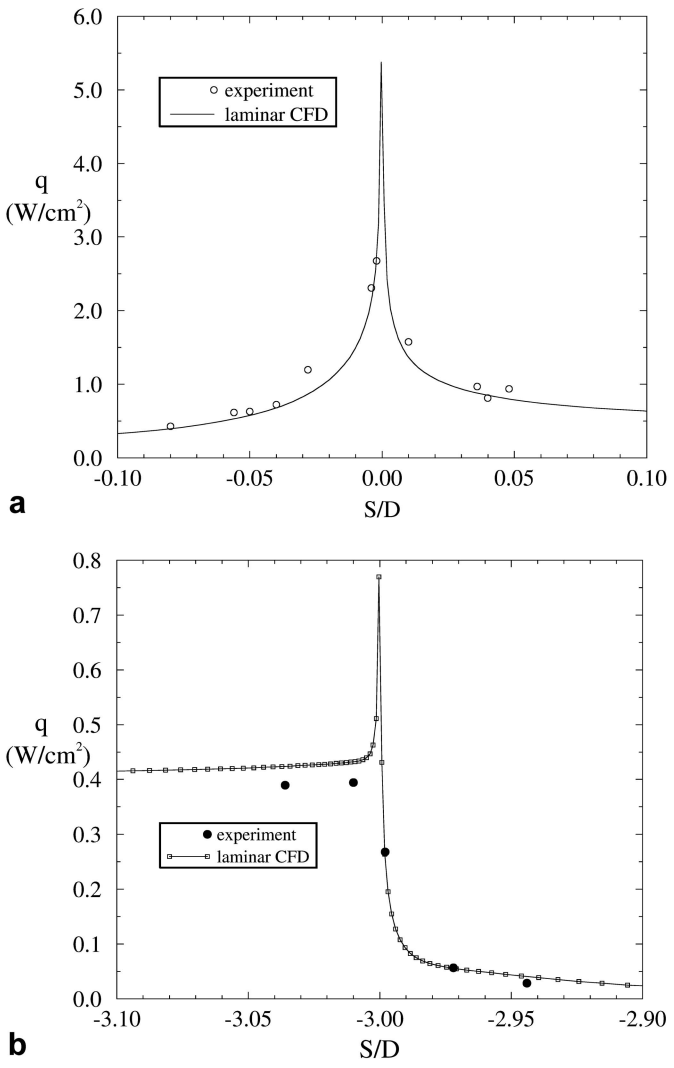

Fig. 8a,b. As for Fig. 7. Localised comparison for data in vicinity of **a** 'reattachment' lip and **b** 'separation' lip

and the upstream or 'separation' lip is at $S/D = -3$ and the downstream or 'reattachment' lip is at $S/D = 0$. The experimental data are an accumulation of measurements at four locations around the circumference, clearly showing that axisymmetry of the mean data is established to a high precision. Measuring such low heat transfer rates is a challenging task in itself, but the comparisons also identify some special flow features and potential difficulties for flow modelling and experiment. It was the CFD in the first instance that forced us to locate gauges exceptionally close to the 'separation' (Fig. 8b) and 'reattachment' (Fig. 8a) lips of the cavity, since these are regions of very rapid variation. The figures identify the narrow spike at shear layer impingement ($S/D = 0$), and also the Goldstein-type singularity (Goldstein 1930) at the forward 'separation' lip ($S/D = -3$). The only region of discrepancy between experiment and CFD is on the cavity floor however ($-2.0 \leq S/D \leq -1.0$ in Fig. 7a), a difference of more than a 2:1 ratio at the maximum. At first in the study this was believed either to result from inadequate mesh resolution, on the one hand, or inaccuracies in measuring such low heat transfer, on the other. Both of these were eliminated by extensive assessments of meshing and measurement accuracy. Similarly, all the evidence experimentally was that the flow field was laminar – certainly transition only occurred a substantial distance downstream of the cavity – so that the mismatch between the *laminar* CFD result and experiment is not believed to be due to the development of turbulent flow. The discrepancy is now believed (Jackson et al. 2001) to be a consequence of three-dimensional laminar instability in the cavity, referred to later in this paper.

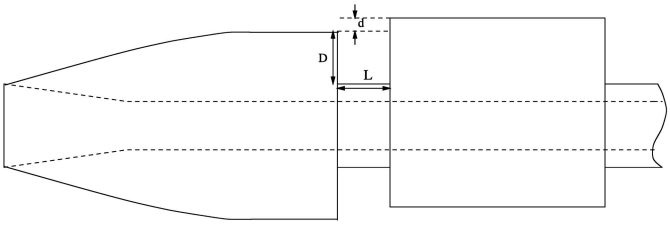

Fig. 9. Schematic for the three-dimensional cavity geometry.

4.3 Design for three-dimensional cavity flows (low unit Reynolds number case)

In the previous section we saw that axisymmetry was established, in the mean, to a very high level of accuracy indeed. A natural way to establish a controlled *three-dimensional* cavity flow therefore was by a *graduated* offset of the afterbody (Jackson et al. 1999), as shown schematically in Fig. 9. Mechanically this was achieved by an eccentric axis arrangement for the afterbody/collar/sting system, so that appropriate rotation enabled it to vary smoothly from axisymmetric to strongly asymmetric. This also means that the minimum amount of instrumentation, usually the most expensive and time-consuming part of model manufacture, can be used to provide a complete effective coverage by relative rotation/movement of modules. Our *initial* modelling (for model design purpose) of the offset case (again the experiments indicated that fully laminar flow is maintained so that the CFD was restricted to laminar modelling) assumed that the flow was 'quasi-two-dimensional', computing a 'local' axisymmetric flow in various azimuthal planes, taking account of the appropriate 'local' changes in afterbody diameter. This is reasonable for the 'weakly' three-dimensional flows, but for strong interactions a full three-dimensional simulation is required. Results of such a full simulation are shown in Fig. 10 providing projections of particle paths in various azimuthal planes. This case corresponds to the same cavity length presented in the previous section but now with an offset, d, of 10% of the cavity depth, D. Figure 11 compares CFD and experiment for the azimuthal variation of the *maximum* heating on the cavity floor. The very low levels for 180 degrees in azimuth are a consequence of the virtually stagnant flow shown in Fig. 10c, in contrast to the more vigorous vortex motion in Fig. 10a,b.

4.4 Design for three-dimensional shock-separated boundary layers (high unit Reynolds number case)

From a recent review of shock-wave/boundary-layer interactions (Dolling 2001) it is clear that the number of well-defined three-dimensional interaction studies is still limited, although this really is the case of practical engineering interest. It is in essence this problem that we are beginning to address. Again, therefore, our studies are all configured to provide both a precise two-dimensional (in the mean) reference flow field and also a *controlled* three-dimensional interaction. In the same manner as the offset cavity study, it is intended to provide a *graduated* variation from fully two-dimensional flows, through 'mildly' three-dimensional to 'strongly' three-dimensional. This is intended both to aid the interpretation of flow physics and also to provide a possible bridge between the relative cheapness of two-dimensional CFD simulations and the very considerable effort involved in a full well-resolved simulation of a highly three-dimensional interaction. In each case a hollow cylindrical forebody generates the axisymmetric test boundary layer. A reference axisymmetric separation is then provided either by a concentric cowl (for impinging shock wave separation), or by a concen-

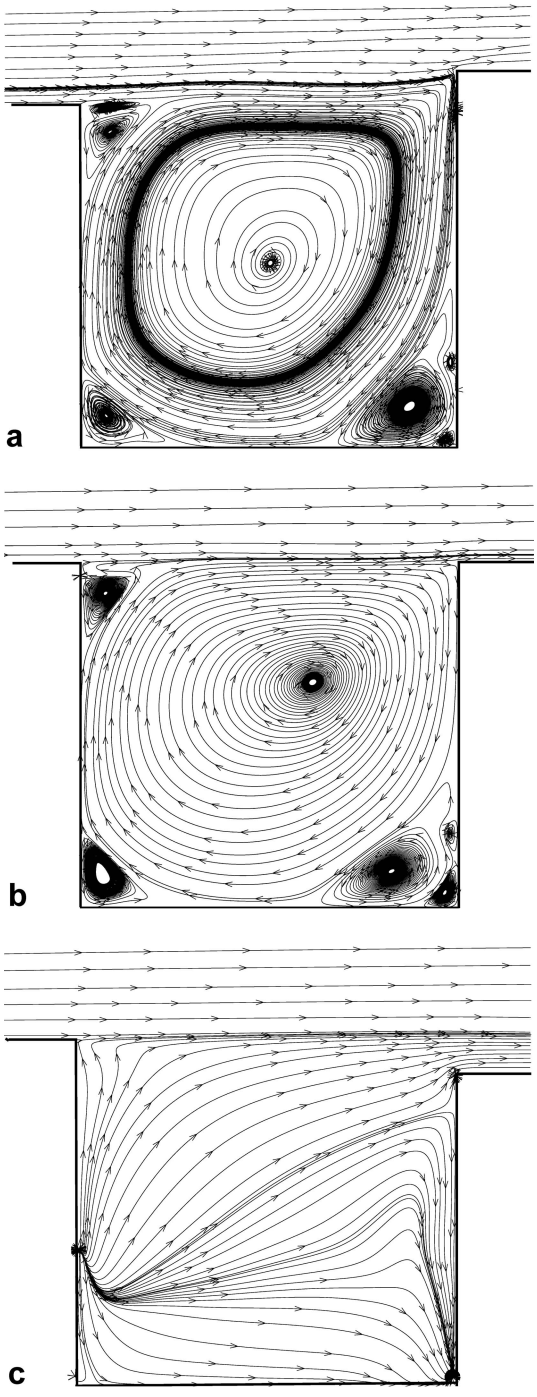

Fig. 10a–c. Particle paths for the offset cavity. **a** 0 degrees, **b** 90 degrees and **c** 180 degrees in azimuth

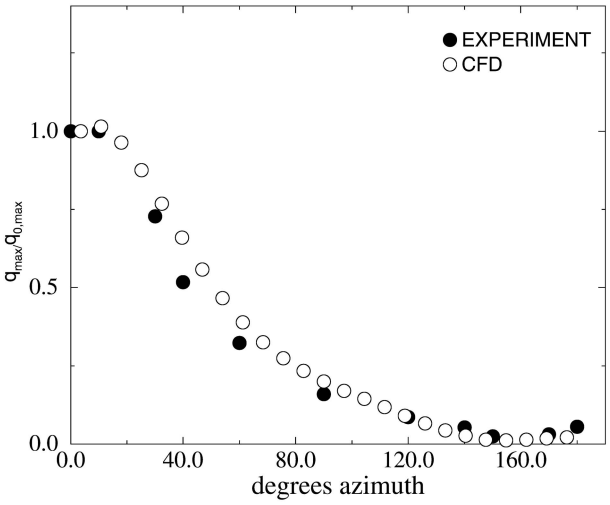

Fig. 11. Three-dimensional cavity. Variation of maximum heat transfer on the cavity floor with azimuthal angle

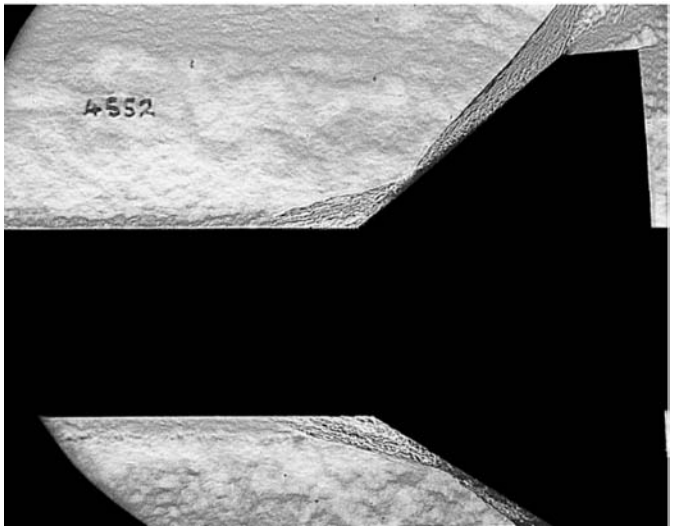

Fig. 12. Schlieren for offset flare configuration. Forebody diameter is 75 mm; the flare semi-angle is 36 degrees and the flare axis is pitched at 4 degrees

tric flare, both of which can then be offset to produce the three-dimensional flow. Other basic three-dimensional separation studies in the literature include yawed, impinging shock waves or yawed surface-mounted wedges (Panaras 1996, Knight et al. 1992, Settles et al. 1986, Kussoy et al. 1980) and the offset flare configuration has also been utilised elsewhere (Brown et al. 1988, Wideman et al. 1995, Gaitonde et al. 1997). Some results for the offset cowl study have already been reported (Boyce and Hillier 2000). As yet our three-dimensional solver is only effectively working for laminar flows, so that configuration development is largely based on prototype tunnel tests. Figure 12, for example, shows schlieren visualisation for an offset flare. Flares can be offset such that their axis is still parallel to that of the forebody (Brown et al. 1988, Wideman et al. 1995, Gaitonde et al. 1997), but for our tests we have pitched a 36 degree semi-vertex angle cone at 4 degrees, to present maximum and minimum deflection angles of 40 degrees (top) and 32 degrees (bottom). Practically, this allows us to minimise the instrumentation, in the same manner as for the 3D cavity flow; the flare is able to rotate around its own axis, whilst keeping the forebody stationary, so that a single stream-wise row of instrumentation along a flare can be used, in successive runs, to provide a full surface coverage. As an interesting preliminary observation we see that, if anything, the total flow separation length on the bottom side is larger than that on the top. From a purely quasi two-dimensional approach, treating each azimuthal plane as if it were a local axisymmetric configuration, the 40 degrees surface would generate a very substantial separation whereas the 32 degrees surface would essentially be an incipient separation case.

4.5 Flow establishment times

Study of flow separation in short-duration facilities is constrained by the issue of flow establishment times. This has been of considerable concern over the years (Holden 1971, Ihrig and Korst 1963, Mallinson et al. 1997, Rom 1963) and has been one of the factors in our CFD design. Establishment of separated regions is controlled by acoustic wave propagation, flow convection and viscous diffusion and since the latter is generally the slowest physical process heat transfer time-histories are probably good indicators of the establishment process. All our test models, where possible, have been subject to CFD simulations of starting processes, irrespective of whether or not the flow will separate. The cowl-centrebody pressure-gradient design, for example, 'stalls' at large pressure ratios, defining one of the operating domain boundaries in Fig. 3, so that flow starting was comprehensively assessed by CFD, plus simple, prototype experiments. Figure 13 is part of our CFD exercise in assessing flow establishment times for the two-dimensional cavity flows, which in turn helped to determine the permitted, maximum cavity scale. In this case a plausible CFD representation was used for the start-up flow in the gun tunnel nozzle. The Mach 9 nozzle flow is established in less than 0.5 ms, and the simulated start incorporated this rapid transient together with a longer time-scale total pressure increase (as measured experimentally at the nozzle inlet) combined with an inferred history for the total temperature. Figure 13a shows computed pressure, skin friction and heat transfer histories, normalised by their steady state values, at a sample position on the cavity floor compared (Fig. 13b) with the actual measured surface pressure history. It is these data that implied that the cavity depth, D, of 25 mm was the largest permissible for this study. One potential problem in defining high quality axisymmetric flows (Jackson et al. 2001) is also revealed by Fig. 14. Figure 14a shows the measured surface heat transfer history, taken as 2.5 ms running-averages that are also further averaged over three identically triggered runs. This indicates that the data achieved a stationary state, and there is also ample evi-

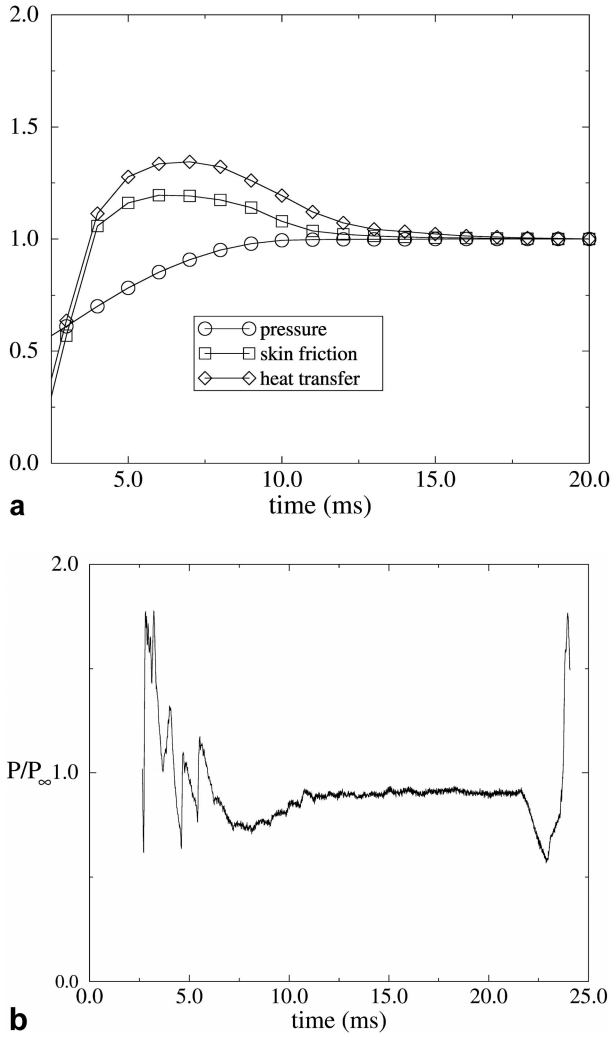

Fig. 13. **a** CFD simulation of cavity flow establishment time, from sample position at mid-chord of the cavity floor. **b** measured pressure starting history at the same location

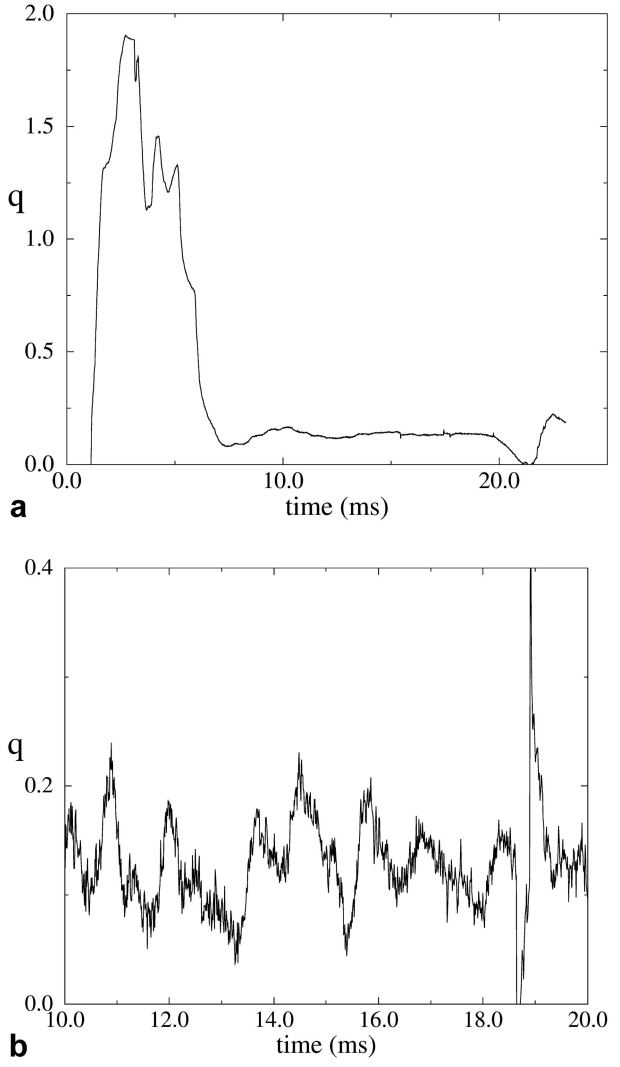

Fig. 14a,b. Experimental heat transfer data at mid-chord of the cavity floor. **a** 2.5 ms running average, taken over several runs. **b** Time-record for one sample run.

dence presented earlier that the *mean* flow is axisymmetric within measurement accuracy. Figure 14b shows a single time record of heat transfer at the same location on the cavity floor, however. This is obviously unsteady, at such a low frequency that it cannot correspond to any of the 'vorticity-shedding' cavity modes (noted for example in Morgenstern and Chokani 1994, Zhang et al. 1998, Tam et al. 1996). It is believed to correspond to an unsteady Goertler-type streamwise vortex structure in the cavity. Ample documentation exists for similar phenomena in low speed, lid-driven cavity flows (Aidun et al. 1991, Ramanan and Homsy 1994), at comparable Reynolds numbers and similar (scaled) frequencies.

5 Concluding remarks

In this paper we have briefly presented a range of configurations that both provide fundamental 'building blocks' in the development of the understanding of high speed flows and also demonstrate a useful partnership between CFD and experiment. In our particular case the cost of experiments is so high that we really endeavour to get our design decisions correct the first time, both for the general configuration shape and also in the detail of the location of instrumentation. The bulk of our models have therefore usually had an intensive CFD exploration before commitment to manufacture.

Acknowledgements. This work has been supported by the Defence Evaluation and Research Agency (now QinetiQ), the Engineering and Physical Sciences Research Council and through the Anglo-Australian Fellowship scheme of the Royal Academy of Engineering and the Royal Society. We gratefully acknowledge this support.

References

Aidun CK, Triantafillopoulos NG, Benson JD (1991) Global stability of a lid-driven cavity with throughflow: flow visu-

alisation studies. Phys Fluids A3:2081–2093
Baldwin BS, Barth TJ (1990) A one-equation turbulence model for high Reynolds number wall bounded flows. NASA TM102847
Baldwin BS, Lomax H (1978) Thin layer approximation and algebraic model for separated turbulent flows. AIAA78-257
Boyce RR, Hillier R (2000) Shock-induced three-dimensional separation of an axisymmetric hypersonic turbulent boundary layer. AIAA 2000-2226
Brown JD, Brown JL, Kussoy MI, Holt M, Horstman CC (1988) Two-component LDV investigation of three-dimensional shock/turbulent boundary-layer interactions. AIAA J 26:52–56
Cook WJ, Felderman EJ (1966) Reduction of data from thin–film heat–transfer gauges: a concise numerical technique. AIAA J 4:561–562
Donovan JF, Spina EF, Smits AJ (1994) The structure of a supersonic turbulent boundary layer subjected to concave surface curvature. J Fluid Mech 259:1–24
Dolling DS (2001) Fifty years of shock-wave/boundary layer interaction research: What next? AIAA J 39:1517–1531
Fernando EM, Smits AJ (1990) A supersonic turbulent boundary layer in an adverse pressure gradient. J Fluid Mech 211:285–307
Gaitonde D, Shang JS, Edwards JR (1997) Structure of a supersonic three-dimensional/offset-flare turbulent interaction. AIAA J 34:294–302
Goldberg UC, Ramakrishnan SV (1994) A pointwise version of the Baldwin-Barth turbulence model. Int J Comp Fluid Dynamics 1:321–338
Goldstein S (1930) Concerning some solutions of the boundary layer equations in hydrodynamics. Proc Camb Phil Soc 26:18–30
Hasan RGM, McGuirk JJ (2001) Assessment of turbulence model performance for transonic flow over an axisymmetric bump. Aero J 105:17–31
Hillier R, Kirk D, Soltani S (1995) Navier-Stokes computations of hypersonic flows. Int J Num Meth Heat & Fluid Flow 5:195–211
Holden M (1971) Establishment time of laminar separated flows. AIAA J 9:2296–2298
Ihrig HK, Korst HH (1963) Quasi-steady aspects of the adjustment of separated flow regions to transient external flows. AIAA J 1:934–937
Jackson AP, Hillier R, Soltani S (1999) A study of two- and three-dimensional separation at hypersonic speeds. In Ball GJ, Hillier R, Roberts GT 22nd Int. Symp. on Shock Waves, University of Southampton, pp 1571–1576
Jackson AP, Hillier R, Soltani S (2001) Experimental and computational study of laminar cavity flows at hypersonic speeds. J Fluid Mech 427:329–358
Keyes FG (1952) The heat conductivity, viscosity, specific heat and Prandtl numbers for thirteen gases. Massachussetts Institute of Technology, Project Squid, Tech Report 37
Knight DD, Horstman CC, Bogdonoff S (1992) Structure of supersonic turbulent flow past a swept compression corner. AIAA J 30:890–896
Kussoy MI, Horstman CC, Acharya M (1978) An experimental documentation of pressure gradient and Reynolds number effects on compressible turbulent boundary layers. NASA TM 78488
Kussoy MI, Viegas JR, Horstman CC (1980) Investigation of a three-dimensional shock wave separated turbulent boundary layer. AIAA J 18:1477–1484
Laderman AJ (1980) Adverse pressure gradient effect on supersonic boundary layer turbulence. AIAA J 18:1186–1195,
Mallinson SG, Gai SL, Mudford NR (1997) Establishment of steady separated flow over a compression-corner in a free piston shock tunnel. Shock Waves 7:249–253
Mallinson SG, Hillier R, Jackson AP (1999) Turbulence modelling of hypersonic turbulent boundary layer flows. In Ball GJ, Hillier R, Roberts GT 22nd Int. Symp. on Shock Waves, University of Southampton, pp 1519–1524
Mallinson SG, Hillier R, Jackson AP, Kirk DC, Soltani S, Zanchetta MA (2000) Gun tunnel flow calibration: defining input conditions for hypersonic flow computations. Shock Waves 10:313–322
Menter FR (1997) Eddy viscosity transport equations and their relation to the $k-\epsilon$ model. J Fluids Eng 119:876–884
Morgenstern A, Chokani N (1994) Hypersonic flow past open cavities. AIAA J 32:2387–2393
Oberkampf WL (2000) Design, execution and analysis of validation experiments. Verification and validation in CFD, VKI-lecture series
Panaras AG (1996) Review of the physics of swept-shock/boundary layer interactions. Prog Aero Sci 37:173–244
Patel VC, Rodi W, Scheurer G (1985) Turbulence models for near-wall and low Reynolds number flows: a review. AIAA J 23:1308–1319
Ramanan N, Homsy GM (1994) Linear stability of lid-driven cavity flows. Phys Fluids 6:2690–2701
Rizzi AW, Vos JB (1998) Towards establishing credibility in computational fluid dynamics simulations. AIAA Journal 36:668–675
Rom J (1963) Measurements of heat transfer in separated regions in a shock tube and in a shock tunnel. AIAA J 1:2193–2194
Roshko A, Thomke GJ (1966)Observations of turbulent reattachment behind an axisymmetric downstream-facing step in supersonic flow. AIAA J 4:975–980
Schultz DL, Jones TV (1973) Heat–transfer measurements in short–duration hypersonic facilities, AGARDograph 165
Settles GS, Horstman CC, McKenzie TM (1986) Experimental and computational study of a swept compression corner interaction flowfield. AIAA J 24:744–752
Shyy W, Krishnamurty VS (1997) Compressibility effects in modeling complex turbulent flows. Prog Aero Sci 33:587–645
Smith DR, Smits AJ (1996) A study of the effects of curvature and compression on the behavior of a supersonic turbulent boundary layer. Experiments in Fluids 18:363–369
Tam C-J, Orkwis PD, Disimile PJ (1996) Algebraic turbulence model simulations of supersonic open-cavity flow physics. AIAA J 34:2255–2260
Vos JB, Rizzi AW, Darracq D (2001) Overview of European validation activities in aeronautics. QNET-CFD Network Newsletter (http://www.qnet-cfd.net):17–20
Wideman JK, Brown JL, Miles JB, Ozcan O (1995) Skin-friction measurements in three-dimensional shock-wave/boundary-layer interaction. AIAA J 33:805–811
Wilcox CD (1992) Turbulence modelling for CFD. DCW Industries, La Canada, California
Zhang X, Rona A, Edwards JA (1998) The effect of trailing edge geometry on cavity flow oscillation driven by a supersonic shear layer. Aero J 102:129–136